

## Radiative Rydberg-atom–Rydberg-atom collisions in the strong-field regime

P. Pillet

*Laboratoire Aimé Cotton, Centre National de la Recherche Scientifique II, Batiment 505, F-91405 Orsay Cedex, France*

R. Kachru, N. H. Tran, and W. W. Smith\*

*Molecular Physics Laboratory, SRI International, Menlo Park, California 94025*

T. F. Gallagher

*Department of Physics, University of Virginia, Charlottesville, Virginia 22901*

(Received 17 February 1987)

We describe the experimental observation of the resonant collisional energy transfer  $\text{Na}(ns) + \text{Na}(ns) + qh\nu \rightarrow \text{Na}(np) + \text{Na}[(n-1)p] + (q \pm m)h\nu$  which occurs when the Na atoms in a strong microwave field are tuned in energy with a static field so that the energy resonance  $E_{ns} + E_{ns} = E_{np} + E_{n-1,p} \pm mh\nu$  occurs. We describe our experimental observations and provide a detailed description of a nonperturbative theory which we have developed to explain our observations. The theory is essentially developed in terms of the resonant dipole-dipole collisions between “microwave dressed” atoms. Using an extension of the approach we used previously to describe resonant dipole-dipole collisions in the absence of microwaves, we are able to take into account all the coherences in the problem in a completely straightforward way.

### I. INTRODUCTION

A collision of two atomic or molecular species in which a photon is absorbed or emitted is frequently called a radiatively assisted collision. Such a process, predicted for the first time by Gudzenko and Yakovlenko in 1972,<sup>1</sup> can be characterized as the induced absorption or emission of one photon during a binary collision in the presence of an intense electromagnetic field, causing some change in the electronic structure of both partners. It may also be viewed as emission or absorption of the transient molecule formed in the collision of the two atoms. Thus the process can also be described in the language of line broadening, as has been shown by Gallagher and Holstein.<sup>2</sup> In either case the short duration of the collision, typically  $10^{-12}$  s, implies that to efficiently drive such a transition, i.e., to either stimulate the emission or absorption of a photon, requires an intense radiation field. Thus it is not surprising that the study of such processes has awaited the development of the high-power tunable dye laser, and recent years have seen the development of a variety of laser-induced collisional energy transfer (LICET) experiments.<sup>3–9</sup>

In spite of the high power of pulsed tunable dye lasers, most of the experiments are in good agreement with a perturbation-theory approach, valid for the weak-electromagnetic-field regime, which predicts a linear laser-power dependence of the cross section.<sup>1,2,10–15</sup> Only recently have deviations from a linear power law been observed for high-laser-power densities of  $\sim 10^9$  W/cm<sup>2</sup>, indicating the breakdown of the perturbative approach and the entrance into the strong-field regime.<sup>16</sup> As it is unrealistic to expect increases of orders of magnitude in dye

laser intensities, the prospect of exploring the strong-field regime for such systems does not appear bright.

More recently, experiments analogous to the laser-induced collision experiments have been performed using Na Rydberg atoms and microwave radiation, in which, because of the large dipole moments of the Rydberg atoms, it was possible to observe radiatively assisted collisional energy transfer at microwave power levels of only a few watts per square centimeter.<sup>17</sup>

To develop a more quantitative feeling for this process, let us first consider the resonant dipole-dipole collisional energy exchange between two Rydberg atoms. The energy exchange is probable if the product of the coupling matrix element and the interaction time is 1. For a resonant dipole-dipole collision this leads to

$$\frac{\mu_1 \mu_2}{b^3} \frac{b}{v} \sim 1, \quad (1)$$

where  $\mu_1$  and  $\mu_2$  are the dipole moments of the transitions in the two atoms,  $b$  is the impact parameter, and  $v$  is the collision velocity. The cross section  $\sigma$  is roughly given by  $\pi b^2$  for the value of  $b$  satisfying Eq. (1). Thus,

$$\sigma = \frac{\mu_1 \mu_2}{v}. \quad (2)$$

Now let us consider the case in which a photon is absorbed or emitted during the collision. In this case the criterion of Eq. (1) is replaced by

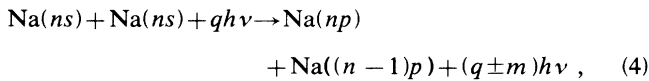
$$\frac{\mu_1 \mu_2 \mu_3}{\Delta b^3} E \frac{b}{v} \sim 1. \quad (3)$$

Here,  $\mu_3$  is the dipole matrix element making the connec-

tion to a third state and  $\Delta$  is an energy detuning. It is clear that the difference between Eqs. (1) and (3) is simply the factor  $\mu_3 E/\Delta$ . If this factor is  $\sim 1$  then the radiatively assisted collision of Eq. (3) is as likely as the resonant collision of Eq. (1).

The large matrix elements and small detunings of the Rydberg states suggest that this should occur for  $E \sim 30$  V/cm for  $n=20$ , which corresponds to a power level of a few watts per square centimeter. As it is straightforward to produce kW/cm<sup>2</sup> power levels, it is in fact possible to reach the strong-field regime using Rydberg atoms and microwave fields.<sup>18</sup>

Specifically, we have studied the microwave-multiphoton-assisted radiative collision process:



where  $m(0 \leq m \leq 4)$  is the number of microwave photons ( $h\nu$ ) emitted or absorbed during a collision. This is depicted in Fig. 1 for  $m=3$ .  $q$  indicates that the collisional process occurs in the presence of  $q$  microwave photons and that the phenomenon is induced by microwave radiation. This process is sharply resonant and occurs when the Rydberg levels are tuned with a static electric field  $F$ , so that

$$E_{np}(F) - E_{ns}(F) \pm mh\nu = E_{ns}(F) - E_{(n-1)p}(F), \quad (5)$$

where  $E_{nl}(F)$  is the energy of the  $nl$  state in the field  $F$ , as shown schematically by Fig. 2 for  $n=18$  in the restrictive case of azimuthal angular momentum quantum number  $|m_l|=0$ . In fact, for each microwave-multiphoton-assisted radiative collision process, there are four collisional resonances due to the splitting of the  $np$  and  $(n-1)p$   $|m_l|=0$  and 1 levels in the electric field, as shown by Fig. 3. We shall designate the different resonances of the  $m$ -photon-assisted collisions by the  $|m_l|$  value of the final lower, then upper,  $p$  levels, respectively, with  $m$  as a superscript. For instance, in order of increasing electric field we label the four one-emitted-photon resonances as  $(0,0)^1$ ,  $(1,0)^1$ ,  $(0,1)^1$ , and  $(1,1)^1$ .

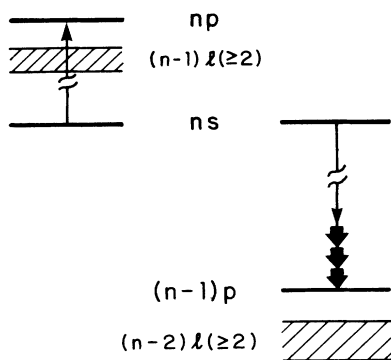


FIG. 1. Energy-level diagram, relevant to the three-emitted-microwave-photon-assisted radiative collision.

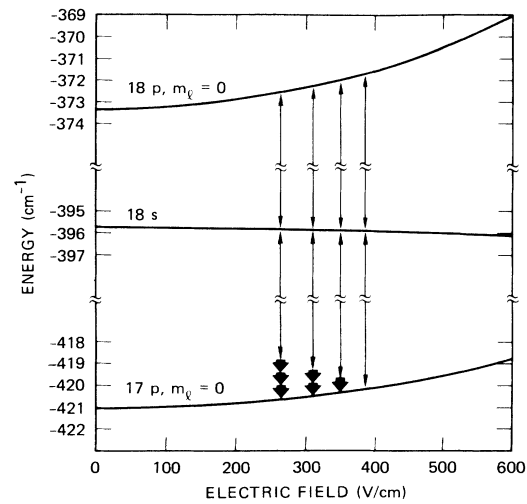


FIG. 2. Stark energy-level diagram of the  $|m_l|=0$  states, relevant to the multiphoton-assisted collisions. The vertical lines indicate the collisional transfer and are drawn at the fields where they occur. The thick arrows correspond to the emitted or absorbed photons.

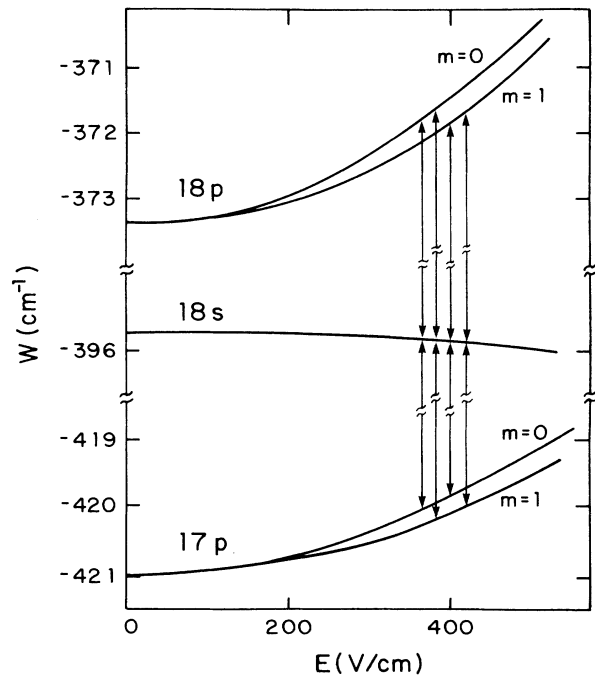


FIG. 3. Energy-level diagram for  $17p$ ,  $18s$ ,  $18p$  states in a static electric field. The vertical lines are drawn at the four fields where the  $s$  state is midway between the two  $p$  states and the resonance collisional transfer occurs. Similar sets of four lines would be drawn for each multiphoton-assisted radiative collision process.

It is our purpose in this paper to give a more complete description and analysis of our experiments as well as a theoretical approach for the interpretation of the experimental data. In Sec. II of this paper we describe the experimental approach for the observation of microwave-assisted radiative collisions. We study the characteristics, such as the cross section, shift, and shape of these resonances, versus the microwave power. Systematic data have been taken for the case of initial excitation to the  $18s$  level and a 15.4-GHz microwave frequency. Survey data for  $17s$  to  $22s$  levels, and for 12.8-, 14.1-, and 15.4-GHz frequencies have also been taken. Cases in which microwave photons are absorbed have also been observed, but the proximity of  $n-1$  and  $n-2$  manifolds to the  $p$  levels leads to supplementary resonances which makes a quantitative investigation difficult.<sup>19</sup> In Sec. III, we give a theoretical description of Rydberg atoms in the presence of microwaves in the low-frequency or adiabatic approximation. We apply this approach to the treatment of radiative collisions in the cases of weak- and strong-field regimes and we give a brief survey of the role of the frequency. Finally, we compare the theoretical results with the experimental data.

## II. EXPERIMENTS

### A. Experimental procedure

Rydberg atoms present many coincidences of energy-level separations because of the systematic variation of energy with principal quantum number  $n$  and orbital angular momentum quantum number  $l$ . The study of resonance effects in collisions is thus greatly facilitated by the use of Rydberg atoms.<sup>20-24</sup> Furthermore, because of the large dipole moments of Rydberg atoms, the application of a very modest electric field shifts their energies and allows the study of resonant collisions with continuous tuning.<sup>23-25</sup> Specifically, the sharply resonant thermal-collision process  $\text{Na}(ns) + \text{Na}(ns) \rightarrow \text{Na}(np) + \text{Na}(n-1p)$ , which occurs when the  $ns$  level lies midway between the two  $p$  states, has been studied, and studies of microwave-assisted radiative collisions<sup>17,18</sup> quite naturally followed these resonant collision experiments.<sup>23,24</sup>

The experimental approach we have used is laser excitation of Na atoms in a beam. An overall diagram of the apparatus is shown in Fig. 4, and a more detailed view is shown in Fig. 5. A thermal beam of Na atoms, provided by an effusive source, passes into a microwave cavity where the atoms are excited by a two-step process, first from the  $3s$  ground state to the  $3p$  state, then, after a 7 ns delay, to a high-lying  $ns$  state using two 5-ns-duration dye laser pulses of wavelengths 5890 and 4150 Å. The laser excitation and subsequent collisions occur in a dc electric field, which ranges from 80–800 V/cm, and in a microwave field of amplitude between 0 and 300 V/cm. At a variable time (of the order of 1–2  $\mu\text{s}$ ) after the laser excitation, a positive high-voltage pulse (of rise time 300 ns) is applied to a septum in the center of the microwave cavity (see the detailed view of the microwave cavity in Fig. 5), which allows us to selectively ionize the Rydberg atoms and to accelerate the resulting ions into an electron

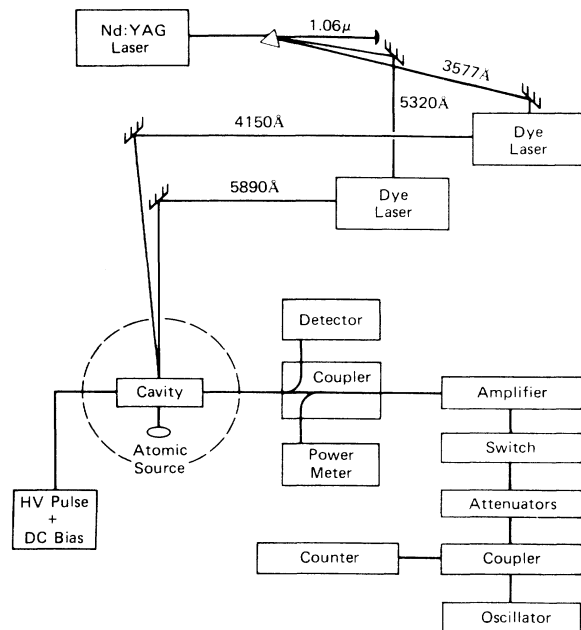


FIG. 4. An overall diagram of the apparatus showing the lasers, the microwave equipment, and the atomic-beam apparatus (HV denotes high voltage, YAG denotes yttrium aluminum garnet).

multiplier. The electron multiplier signal is averaged using a boxcar averager, then recorded with an  $x$ - $y$  recorder.

The entire apparatus used in the experiments is described elsewhere,<sup>25-26</sup> and a complete description of the microwave cavity can be found in Ref. 26. Nevertheless, we note here the points of particular importance for these

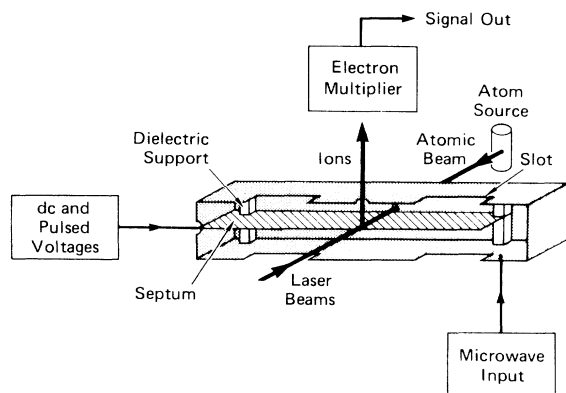


FIG. 5. Main features of the atomic-beam apparatus, the atomic source, the microwave cavity, and the electron multiplier. The microwave cavity is shown sliced in half. The copper septum bisects the height of the cavity. Two holes of diameter 1.3 mm are drilled in the side walls to admit the collinear laser and Na atomic beams, and a 1-mm hole in the top of the cavity allows  $\text{Na}^+$  resulting from field ionization of Na to be extracted. Note the slots for pumping.

experiments. A thermal Na beam moves slowly ( $\sim 10^5$  cm/s), thus the Rydberg atoms do not move more than 1 mm during the  $1 \mu\text{s}$  time during which the experiment takes place. As a result, we must be able to produce a tunable static electric field, a strong ionizing electric field pulse, and a microwave field, all spatially homogeneous over the region occupied by the Rydberg atoms under study. These considerations have led to the design of the cavity of Fig. 5, which is a derivative of the techniques used in microwave Stark spectroscopy, i.e., putting a septum inside a piece of rectangular waveguide.<sup>27</sup> As used in these experiments, the cavity had a  $Q$  of 1400, so that an incident power of 1 W at 15.4 GHz produced a field at the location of the observed atoms of 95 V/cm. The applied ionizing field amplitude is just enough to ionize selectively the  $np$  level but not the  $ns$  or  $(n-1)p$  levels and enables us to detect selectively the population of the  $np$  level when the field-ionizing pulse is applied.

### B. Observations and main characteristics

The most striking feature of our observations is the sharply resonant increase in the populations of  $p$  levels when the levels are tuned into the resonance condition of Eq. (4) with the field, as shown in Fig. 2. This can occur with the stimulated emission of 0,1,2,3,... photons as shown by Fig. 2. Before considering the case of multiphoton emission, the strong-field regime, it is useful to examine the single-photon radiatively assisted collisions which roughly correspond to previous LICET experiments.<sup>28</sup> We show in Fig. 6 the collisional resonances corresponding to  $\text{Na}(22s) + \text{Na}(22s) + qh\nu \rightarrow \text{Na}(22p) + \text{Na}(21p) + (q+m)h\nu$  for  $m=0$  and 1, i.e., the normal resonant collisions and the single-photon radiative collision. Specifically, the signals shown in Fig. 6 are the  $22p$  signals observed when populating the  $22s$  state with the lasers and scanning the static field. As shown by Fig. 6, the single-photon-assisted collision signal is roughly as

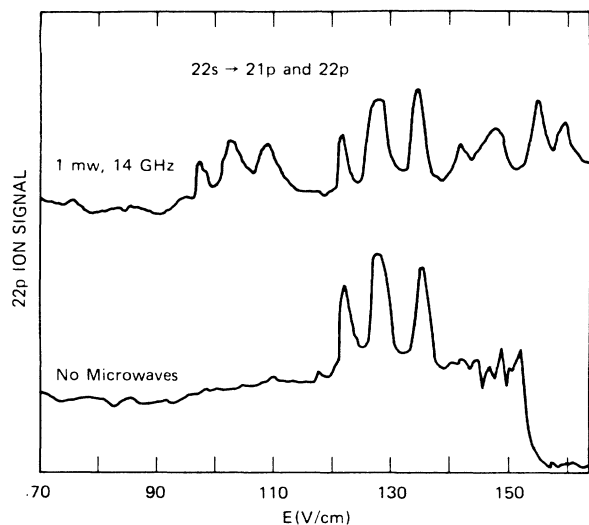


FIG. 6. Observed  $22p$ -ion signal after the population of the  $22s$  level, with and without 1 mW of 14 GHz microwave power.

large as the resonant collision signal. The microwave field is thus no longer a small perturbation, and we are on the verge of the strong-field regime. Even at the low microwave power of  $\langle 1\text{mW}$ , corresponding to a microwave field of 3 V/cm, we have a situation comparable to a LICET experiment with a laser intensity of  $\sim 10^9$  W/cm<sup>2</sup>.

As the microwave power can easily be raised by four orders of magnitude, it is possible to go well into the strong-field regime. A good example is the development of the process  $\text{Na}(18s) + \text{Na}(18s) \rightarrow \text{Na}(18p) + \text{Na}(17p) + mh\nu$  with 15.4 GHz microwave power. We have studied this case in some detail, and in Fig. 7 we show a series of recordings at increasing microwave powers which illustrates the development with microwave power. The data of Fig. 7 are those obtained by populating the  $18s$  level and recording the  $18p$ -level population signal as the static field is swept. Figure 7(a) corresponds to the case without microwaves ( $m=0$ ) and shows the four zero-photon resonant collision peaks. As the microwave power is increased, Figs. 7(b), 7(c), and 7(d) each show the appearance of sets of four new peaks corresponding, respectively, to the one-, two-, and three-microwave-emitted-photon-assisted resonant collisional energy transfers, as shown in Fig. 2. We indicate in Fig. 7 the  $(0,0)^m$  resonances by the number  $m$  and an arrow.

Before describing or interpreting our observations in great detail it is worth noting the salient characteristics of our observations. First, due to the strength of the dipole-dipole collisional interaction it is easily possible to equilibrate the populations of the  $ns$ ,  $np$ , and  $(n-1)p$  states, especially for the zero-photon collision process in which case the  $np$  population is linear in the number of  $ns$  atoms produced, not quadratic. Thus some care must be exercised in making quantitative measurements of cross sections. Second, for all the resonances we observe shifts proportional to the incident microwave power  $W_I$  driving the cavity, i.e., the square of the microwave field amplitude inside the cavity. Figure 8 shows the shifts of resonances  $(0,0)^1$ ,  $(0,0)^2$ , and  $(0,0)^3$  versus the incident microwave power  $W_I$  at 15.4 GHz frequency for the process  $\text{Na}(18s) + \text{Na}(18s) \rightarrow \text{Na}(18p) + \text{Na}(17p) + mh\nu$ . Third, we note for each process an evolution from an asymmetrically shaped profile to a symmetrical one. For example, in Fig. 7(b) the one-photon-assisted collisional resonance at 348 V/cm is weak, broad, and very asymmetric, while at the higher power of Fig. 7(c) it is narrower and stronger. We observe identical behavior versus microwave power for the two- and three-photon-assisted collisional resonances at 300 and 253 V/cm [see Figs. 7(c)–7(e)]. This occurs because the radiative-collision-interaction strength depends on both the internuclear separation and the microwave power as shown by Eq. (3). We note also that the zero-, one-, and two-photon processes reach maxima then decrease, even becoming equal to zero in the case of zero- and one-photon signal, as the microwave power is increased. In the case of the zero-photon process, the signal appears again at higher power. These characteristics are summarized by Fig. 9, which shows the variation of the maximum of the signal of  $(0,0)^m$  resonances versus the input microwave power and therefore gives the evolution of experimental cross sections for the

$m$ -emitted-photon-assisted collisions with microwave power.

Finally we note that the data presented for the  $18s$  state and a frequency of 15.4 GHz are typical. This is illustrated by Fig. 10, a series of recordings at different 12.8-GHz microwave powers of the process  $\text{Na}(20s) + \text{Na}(20s) + qh\nu \rightarrow \text{Na}(20p) + \text{Na}(19p) + (q+m)h\nu$ . In this case, 1 W of input power corresponds to a field of 100 V/cm. As shown by Fig. 10 the development with microwave power is similar to the development shown in Fig. 7. At higher

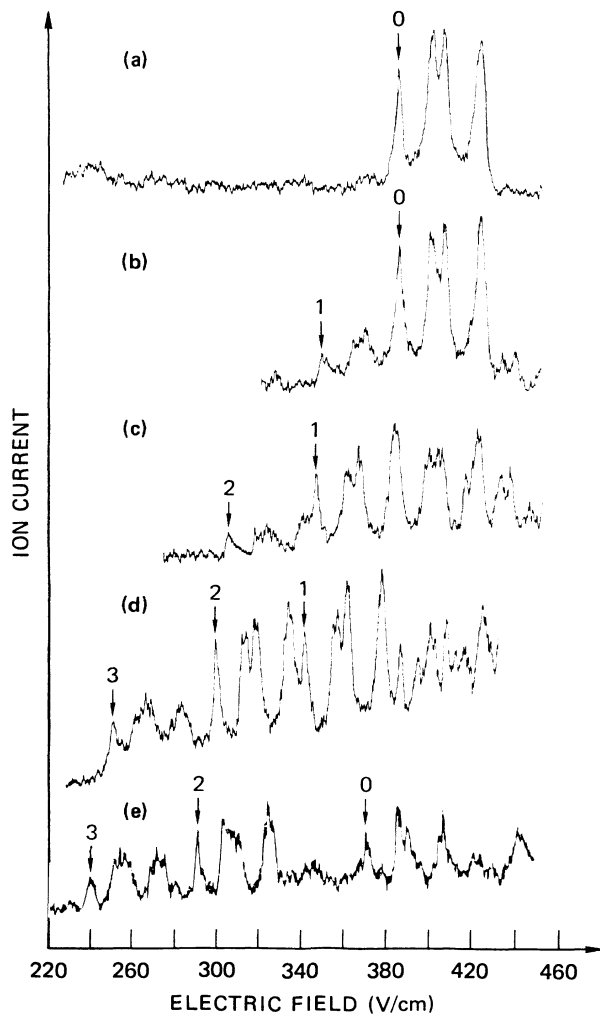


FIG. 7. Observed  $18p$ -ion signal after the population of the  $18s$  level vs the static field with a 15.4-GHz microwave field. Trace (a) corresponds to no microwave power input to the cavity and shows the set of four zero-photon collisional resonances. Traces (b), (c), (d), and (e) correspond, respectively, to 13.5, 50, 105, and 165 V/cm microwave field amplitudes inside the cavity and show additional sets of four collisional resonances corresponding to one-, two-, and three-photon radiatively assisted collisions. The peaks labelled 0, 1, 2, and 3 correspond to the lowest-field member of the set of four resonances corresponding to zero-, one-, two-, and three-photon-assisted collisions,  $(0,0)^0$ ,  $(0,0)^1$ ,  $(0,0)^2$ ,  $(0,0)^3$ .

microwave powers the sets of four resonances corresponding to one-, two-, and three-photon-assisted collisions appear and become stronger, and zero-photon-assisted collision resonances disappear. Again, when a set of resonances first appears they are broad, and they grow narrower with increasing power.

For a detailed examination we have chosen the process  $18s + 18s \rightarrow 17p + 18p$  to have well-resolved collisional resonances and the possibility of having stimulated emission of as many photons as possible. These considerations argue for low  $n$  states, but the microwave power requirements argue for higher  $n$  states. The  $18s$  state is an optimal choice for our experimental constraints. In any event, we observed no significantly different behavior for  $16 < n < 22$  or for frequencies in the 12–15-GHz range, as implied by Fig. 10.

In general these results cannot be explained by an approach in which the microwave field is treated as a perturbation, for such an approach would not predict, for example, the disappearance of the one-photon collisions with increasing microwave power. To interpret these results, we have developed a theory of radiative collisions based on the work of Autler and Townes,<sup>29</sup> which leads to a theory valid in the strong-field regime.

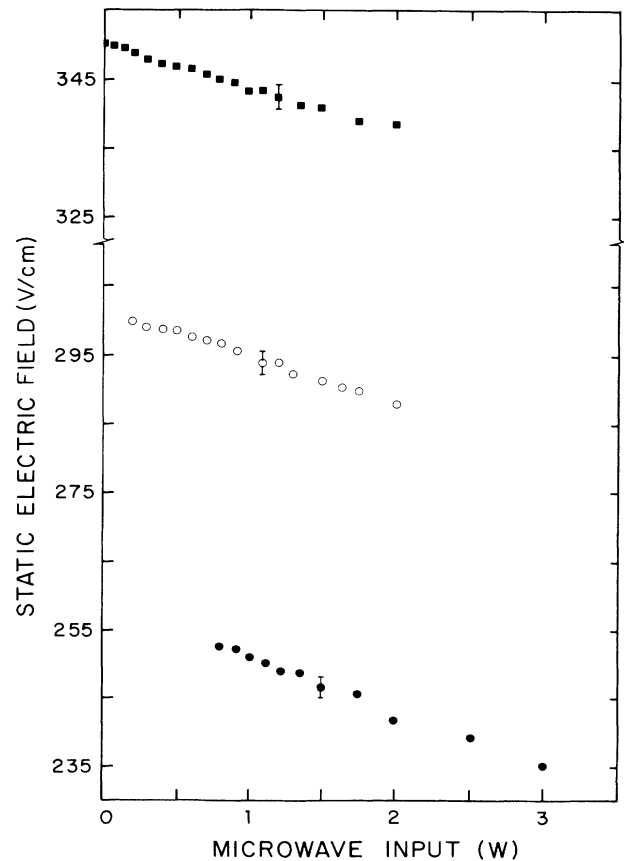


FIG. 8. Experimental field positions of the  $\text{Na}(18s) + \text{Na}(18s) \rightarrow \text{Na}(17p) + \text{Na}(18p) + mh\nu(0,0)^1$  (■),  $(0,0)^2$  (○), and  $(0,0)^3$  (●) microwave-assisted collisional resonances vs 15.4 GHz microwave power. Note the ac Stark shifts of the resonances.

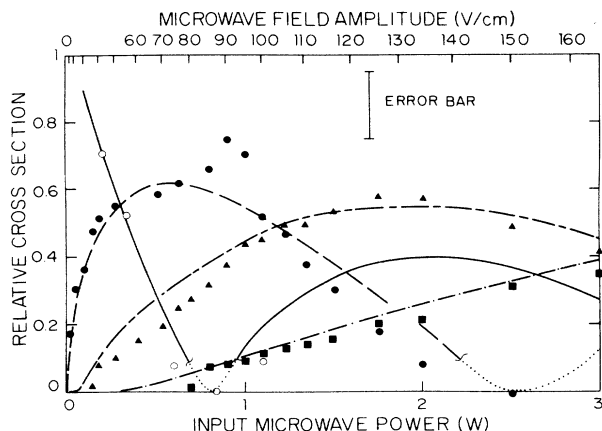


FIG. 9. Variation of the  $(0,0)^m$  measured cross sections with input power at 15.4 GHz for the process  $\text{Na}(18s) + \text{Na}(18s) \rightarrow \text{Na}(17p) + \text{Na}(18p) + mh\nu$ :  $(0,0)^0$  ( $\circ$ ),  $(0,0)^1$  ( $\bullet$ ),  $(0,0)^2$  ( $\triangle$ ), and  $(0,0)^3$  ( $\blacksquare$ ). The experimental points are to be compared to the theoretical cross-section curves  $(0,0)^0$  (—),  $(0,0)^1$  (---),  $(0,0)^2$  (-.-.-),  $(0,0)^3$  (.....). The dotted lines correspond to the part where the theory has not been developed. The experimental and theoretical curves are normalized so that the experimental point (not shown) for the  $(0,0)^0$  resonance with no microwave power has a relative cross section of 2.0. Note that the  $(0,0)^0$  cross section vanishes at an input power of  $\sim 0.8$  W and that the  $(0,0)^1$  cross section vanishes at  $\sim 2.5$  W.

### III. THEORETICAL ANALYSIS

The collisions in the strong-microwave-field regime may be described in terms of collisions of atoms “dressed” by the microwave field. Thus in this section we first treat the effect of the microwave field on a Rydberg atom following the approach of Autler and Townes.<sup>29</sup> Then the resonant collisional energy exchange between the dressed atoms is treated formally. Finally, approximate expressions are developed for both the weak- and strong-microwave-field regimes.

#### A. Rydberg atoms in the presence of a microwave field: The adiabatic approximation

The problem of the effect of a rapidly varying electric field on two states of a quantum-mechanical system has been thoroughly developed by Autler and Townes,<sup>29</sup> and explicit approximate solutions have been obtained for a variety of special cases. The case in which the frequency of the field is low compared to the energy difference between the two states is particularly simple because the problem can be treated quasistatically. This low-frequency approach is particularly well suited to the description of the  $s$  and  $p$  levels of Na Rydberg atoms in the presence of a microwave field. Figure 11 is a Stark diagram of the  $\text{Na } |m_l| = 0$  states around the manifold of  $n = 17$  Stark states. As we can see, the  $s$  and  $p$  levels are separated from the other levels of angular momentum  $l \geq 2$ . The physical implication of the low-frequency ap-

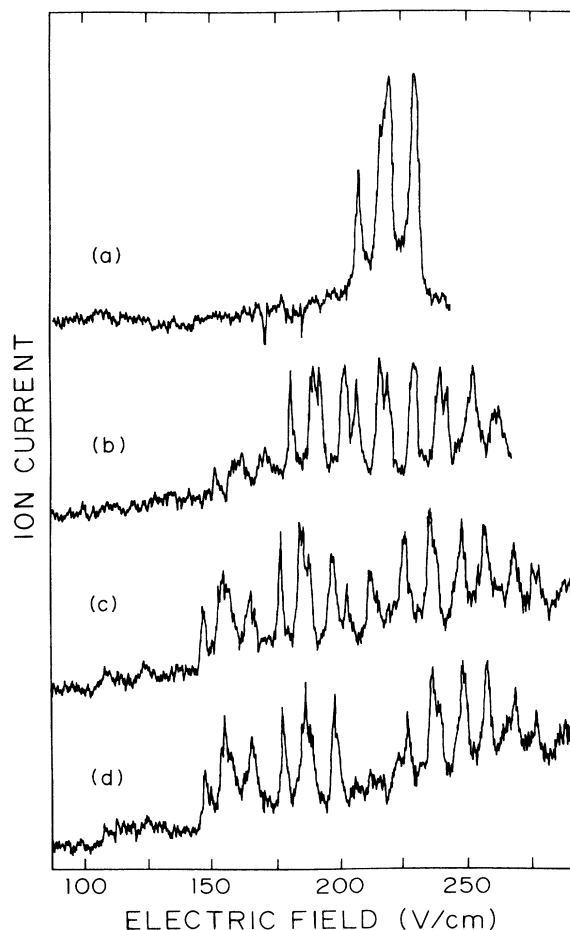


FIG. 10. Observed  $20p$ -ion signal after population of the  $20s$  state. The recordings are taken with (a) no microwaves, (b) 100 mW input power, (c) 300 mW input power, and (d) 400 mW input power. The numbers indicate the  $m$  of the  $(0,0)^m$  collisional resonances. As in Fig. 7, at progressively higher powers, collisions in which more photons are emitted are observed. Also note that the  $(0,0)^0$  resonances vanish for an input power of 400 mW.

proximation is that the atom follows adiabatically the  $s$  or  $p$  level of the Stark diagram as the field oscillates.

In other words, the adiabatic hypothesis means that there is no transition from the  $s$  or  $p$  level to other levels due to the microwaves. Our prior study of 15-GHz microwave ionization of Na Rydberg atoms<sup>26,30</sup> has shown that there is effectively no mixing between  $s$  or  $p$  levels and the  $l \geq 2$  levels of the nearest manifold as long as the microwave field amplitude is insufficient to reach the level crossing where the  $s$  or  $p$  level intersects the manifold. This condition is satisfied here; thus the microwave electric field can be considered as a quasistatic or slowly varying electric field for the  $s$  and  $p$  levels of Na Rydberg atoms. Only the  $s$  and  $p$  states will be explicitly taken into account, the  $l \geq 2$  states entering implicitly through the Stark shifts of the  $s$  and  $p$  levels.

Using the adiabatic approximation we may construct wave functions for the Na  $ns$  and  $np$  states "dressed" by the microwave field.

Explicitly, the wave function of the  $ns$  or  $np$  state  $\phi_{mw}^{nl}$  is given by

$$|\phi_{mw}^{nl}(F)\rangle = \left[ \exp \left[ -i \int_0^t E_{nl}(F(t')) dt' \right] \right] |\phi^{nl}(F)\rangle, \quad (6)$$

where the electric field  $F$  is the sum of a static electric field  $F_s$  and a microwave field of amplitude  $F_{mw}$  and angular frequency  $\omega_{mw}$ :

$$F(t) = F_s + F_{mw} \cos(\omega_{mw}t), \quad (7)$$

$|\phi^{nl}(F)\rangle$  is the spatial wave function of the  $nl$  state in presence of a static field of value  $F$ . The energy and time dependence of the wave function is given by

$$\left[ \exp \left[ -i \int_0^t E_{nl}(F) dt' \right] \right],$$

where  $E_{nl}(F)$  is the energy of the  $nl$  level for a given value  $F$  of the electric field.

By assuming that  $|\phi^{nl}(F)\rangle$  is quasiconstant and by using a limited development of  $E_{nl}$  to second order in the microwave field  $[F_{mw} \cos(\omega_{mw}t)]$ , the wave function  $|\phi_{mw}^{nl}(F)\rangle$  can be written

$$|\phi_{mw}^{nl}(F)\rangle = \left\{ \exp \left[ -i \int_0^t \left[ E_{nl}(F_s) + \frac{dE_{nl}}{dF} \Big|_{F_s} F_{mw} \cos(\omega_{mw}t') + \frac{1}{2} \frac{d^2E_{nl}}{dF^2} \Big|_{F_s} F_{mw}^2 \cos^2(\omega_{mw}t') \right] dt' \right] \right\} |\phi^{nl}(F_s)\rangle, \quad (8)$$

where  $(dE_{nl}/dF)|_{F_s}$  and  $(d^2E_{nl}/dF^2)|_{F_s}$  are the first and second derivatives of the energy  $E_{nl}$  of the state  $nl$  with respect to the field calculated at  $F_s$ . Alternatively,

$$|\phi_{mw}^{nl}(F)\rangle = \left\{ \exp \left[ -i \left[ E_{nl}(F_s) + \frac{1}{4} \frac{d^2E_{nl}}{dF^2} \Big|_{F_s} F_{mw}^2 \right] t \right] \exp \left[ -i \left[ \frac{dE_{nl}}{dF} \Big|_{F_s} \frac{F_{mw}}{\omega_{mw}} \right] \sin(\omega_{mw}t) \right] \right. \\ \left. \times \exp \left[ -i \frac{1}{8} \left[ \frac{d^2E_{nl}}{dF^2} \Big|_{F_s} \frac{F_{mw}^2}{\omega_{mw}} \right] \sin(2\omega_{mw}t) \right] \right\} |\phi^{nl}(F_s)\rangle. \quad (9)$$

Using a Floquet development<sup>29</sup> the wave function may be written

$$|\phi_{mw}^{nl}(F)\rangle = \sum_{m=-\infty}^{+\infty} \sum_{p=-\infty}^{+\infty} (-1)^{m-p} J_{m-2p} \left[ \frac{dE_{nl}}{dF} \Big|_{F_s} \frac{F_{mw}}{\omega_{mw}} \right] J_p \left[ \frac{1}{8} \frac{d^2E_{nl}}{dF^2} \Big|_{F_s} \frac{F_{mw}^2}{\omega_{mw}} \right] \\ \times \exp \left[ -i \left[ E_{nl}(F_s) + \frac{1}{4} \frac{d^2E_{nl}}{dF^2} \Big|_{F_s} F_{mw}^2 - m\omega_{mw} \right] t \right] |\phi^{nl}(F_s)\rangle, \quad (10)$$

which in a first approximation, when  $F_{mw} \lesssim F_s$ , can be written

$$|\phi_{mw}^{nl}(F)\rangle \approx \sum_{m=-\infty}^{+\infty} (-1)^m J_m \left[ \frac{dE_{nl}}{dF} \Big|_{F_s} \frac{F_{mw}}{\omega_{mw}} \right] \exp \left[ -i \left[ E_{nl}(F_s) + \frac{1}{4} \frac{d^2E_{nl}}{dF^2} \Big|_{F_s} F_{mw}^2 - m\omega_{mw} \right] t \right] |\phi^{nl}(F_s)\rangle. \quad (11)$$

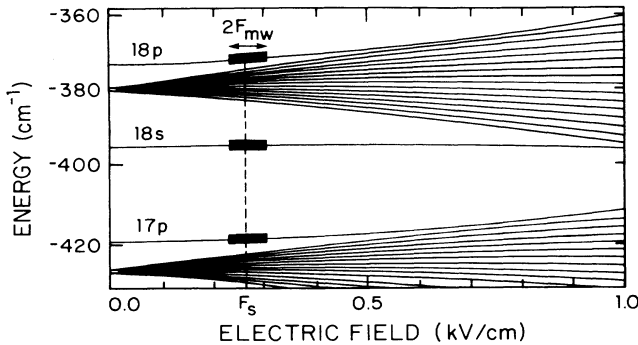


FIG. 11. Stark diagram in the vicinity of the  $n = 17$  manifold. The microwave field of  $F_{mw}$  amplitude creates an oscillation on the  $18p$ -,  $18s$ -, and  $17p$ -level energy curves around the value of the static electric field  $F_s$ .

As shown by Eq. (8), the wave function  $|\phi_{mw}^{nl}(F)\rangle$  of an  $ns$  or  $np$  state in the combination of static and microwave fields is the same spatial wave function  $|\phi_{mw}^{nl}(F_s)\rangle$  as for only the static field  $F_s$ . However, there is no longer a single energy for this wave function but rather a spectrum of sidebands centered around the central energy, and the intensity of each sideband, i.e., how strongly it would appear in a photoabsorption experiment, is given by

$$I^{(m)} = \left| J_m \left[ \frac{dE_{nl}}{dF} \Big|_{F_s} \frac{F_{mw}}{\omega_{mw}} \right] \right|^2, \quad (12)$$

as shown by Fig. 12, and the sidebands are separated by the energy  $\hbar\omega_{mw}$  of one microwave photon. Furthermore, the central frequency is shifted from its energy without microwaves by an amount

$$\Delta E_{nl} = \frac{1}{4} \frac{d^2E_{nl}}{dF^2} \Big|_{F_s} F_{mw}^2 \quad (13)$$

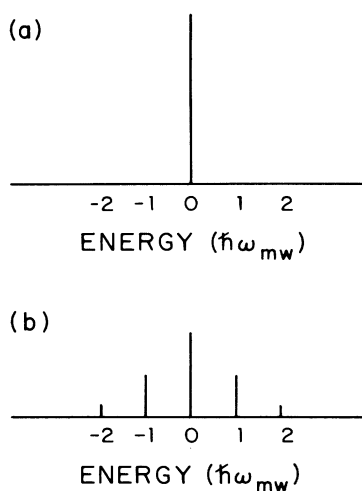


FIG. 12. Theoretical energy spectra of a  $p$  level in a static field, in units of the applied microwave frequency (a) in the absence of microwaves and (b) for a nonzero microwave field amplitude.

proportional to the square of the amplitude of the microwave field.

We can see that only  $p$  levels will acquire significant sideband amplitudes as the  $s$  states have negligible Stark shifts and therefore negligible values of  $dE_{ns}/dF$ . We note also that because of the relatively low values of  $F_s$  and  $F_{mw}$  considered, the  $p$  and  $s$  Stark energies can be adequately approximated by a quadratic field dependence, and the second-order development is adequate. Finally, let us again remark that the theory takes into account all other levels by means of the Stark variation of  $E_{nl}$ .

### B. Long-range dipole-dipole interaction in the presence of microwaves

The theoretical treatment of long-range dipole-dipole collisions has been developed in several places,<sup>31–35</sup> and a description of resonant Rydberg-atom–Rydberg-atom collisions can be found in Ref. 25. A rather similar theory is proposed here incorporating the microwave field in the adiabatic approximation. The essence of our theory is to treat radiative collisions between Rydberg atoms in the presence of a microwave field as resonant collisions between microwave-dressed Rydberg atoms. Consider the collisions in which one photon is emitted. It is clear from Fig. 13 that this process is possible between several pairs of levels of the dressed atom. As we shall see, these processes are coherent and interferences between the different processes appear.

Consider two colliding atoms as shown in Fig. 14. One of the atoms is assumed to be stationary at the origin and the other passing the first atom with an impact parameter  $b$  at  $x=0$  with a relative velocity  $v$  parallel to the  $x$  axis. We assume also, because of the large impact parameter, that the second atom is not deflected by the collision and travels in a straight line. To match our experimental configuration we assume that the static and microwave

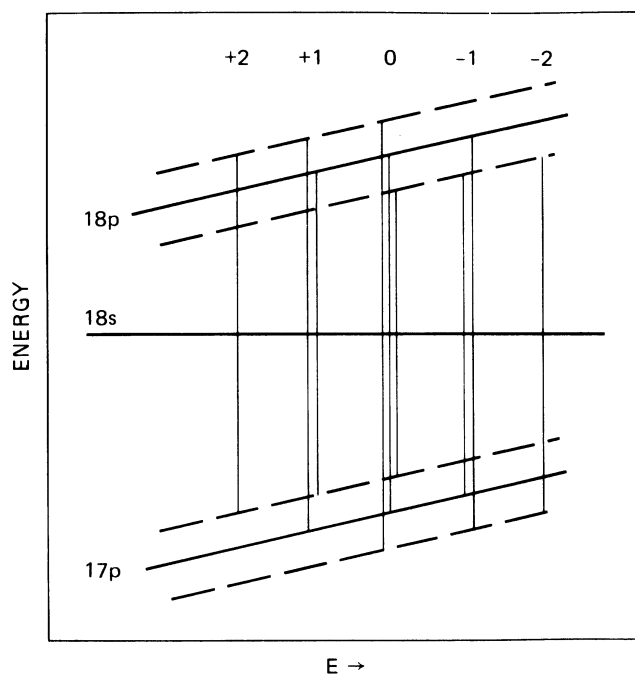


FIG. 13. Energy levels of the  $17p$ ,  $18s$ , and  $18p$  states showing the first upper and lower sideband states of the  $p$  states. The numbers  $+2, \dots, -2$  refer to the net number of photons emitted. Note that there are several processes which lead to the net emission of zero photons, for example.

electric fields  $F_s$  and  $F_{mw}$  are in the  $z$  direction. We construct the product states:

$$|\psi_A(F_s)\rangle = |\phi^{ns}(F_s)\rangle_1 \otimes |\phi^{ns}(F_s)\rangle_2, \quad (14)$$

$$|\psi_B(F_s)\rangle = |\phi^{np}(F_s)\rangle_1 \otimes |\phi^{(n-1)p}(F_s)\rangle_2.$$

Although we shall return to this point later, we note that the energy of the product state  $|\psi_A\rangle$  is twice the energy of the  $ns$  state, and the energy of the product state  $|\psi_B\rangle$  is the sum of the energies of the  $np$  and  $(n-1)p$  states. Consequently, the Stark shift of the state  $|\psi_B\rangle$  is roughly twice the Stark shift of the  $np$  state or  $(n-1)p$  state. As we shall see, using the product states of Eq. (11) takes into account automatically the coherence of the different

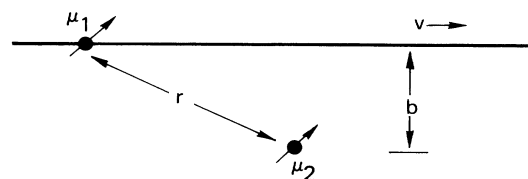


FIG. 14. Geometry of the collision of two dipoles.  $\mu_2$  is at rest and  $\mu_1$  passes with velocity  $v$  and impact parameter  $b$ . The dipoles are separated by  $r$ .

processes shown in Fig. 13. The total wave function for the system may be written as

$$|\psi(t)\rangle = C_A(t)|\psi_A(F_s)\rangle + C_B(t)|\psi_B(F_s)\rangle. \quad (15)$$

The Hamiltonian of the system is given by

$$H = H_0 + V,$$

where  $H_0$  is the Hamiltonian of the two atoms at  $r = \infty$ , where  $r$  is the internuclear separation. Explicitly, we may write

$$H_0 = \begin{bmatrix} W_A & 0 \\ 0 & W_B \end{bmatrix}, \quad (16)$$

with

$$W_A(F(t)) = E_{ns}(F(t)) + E_{ns}(F(t)),$$

$$W_B(F(t)) = E_{np}(F(t)) + E_{(n-1)p}(F(t)),$$

and  $V$  is the long-range dipole-dipole interaction coupling the states  $A$  and  $B$ . For finite internuclear separations,

$$\langle \psi_A | V | \psi_B \rangle = \left\langle \psi_A \left| \frac{\boldsymbol{\mu}_1 \cdot \boldsymbol{\mu}_2}{r^3} - \frac{3(\boldsymbol{\mu}_1 \cdot \mathbf{r})(\boldsymbol{\mu}_2 \cdot \mathbf{r})}{r^5} \right| \psi_B \right\rangle, \quad (17)$$

where  $\mathbf{r}$  is the vector between the two atoms and  $\boldsymbol{\mu}_1(2)$  the dipole vector of the atom 1(2). In this treatment we have only considered the resonant dipole-dipole coupling of Eq. (17) between the two molecular states  $A$  and  $B$ . In fact, there are nonresonant couplings to other molecular states which lead to variations in energy with internuclear separation as shown in Fig. 15. This in turn produces asymmetric collisional resonances, as shown by Figs. 7(a) and 10(a). These asymmetries are not included in the theory.

The interaction matrix elements may be simplified by

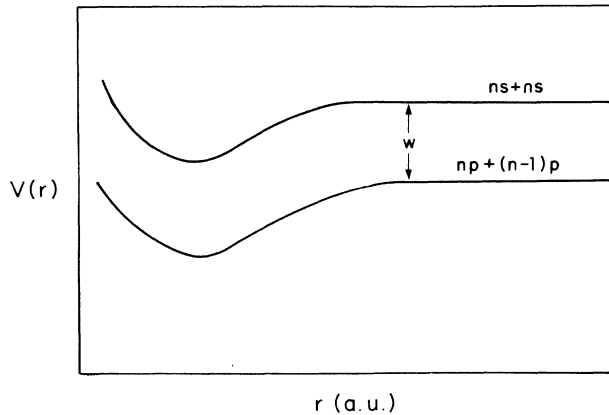


FIG. 15. Microwave-assisted radiative collision in the quasi-molecular point of view. The energies of initial and final states depend on the internuclear separation  $r$  and the collision is, in essence, a photon-induced transition. For weak microwave power, the collision requires smaller impact parameter leading to asymmetrically shaped collisional resonances.

taking the rms value of Eq. (14) over the angle  $\theta$  in Fig. 16. This yields for the  $(0,0)^m$  transition,

$$\langle \psi_A | V | \psi_B \rangle = (\langle ns | \mu_1 | np \rangle \langle ns | \mu_2 | (n-1)p \rangle) / r^3. \quad (18)$$

The evolution equations of the system are given by

$$\begin{aligned} i\dot{C}_A &= W_A C_A + V C_B, \\ i\dot{C}_B &= V^* C_A + W_B C_B. \end{aligned} \quad (19)$$

Initially both atoms are in the  $s$  state, thus  $C_A(-\infty) = 1$  and  $C_B(-\infty) = 0$ . An approximate solution can be calculated by choosing for the matrix element  $V$ :

$$V = \begin{cases} \chi/b^3 & \text{for } -b \leq r \leq b \\ 0 & \text{elsewhere,} \end{cases} \quad (20)$$

with  $\chi = \langle ns | \mu_1 | np \rangle \langle ns | \mu_2 | (n-1)p \rangle$ .

We choose the time origin so that the collision interaction occurs for  $0 \leq t \leq 2b/v$ . By substituting

$$\begin{aligned} C_A(t) &= U_A(t) \exp \left[ -i \int_0^t W_A(t') dt' \right], \\ C_B(t) &= U_B(t) \exp \left[ -i \int_0^t W_B(t') dt' \right] \end{aligned} \quad (21)$$

in Eqs. (19), we can write

$$\begin{aligned} i\dot{U}_A &= V \exp \left[ i \int_0^t [W_A(t') - W_B(t')] dt' \right] U_B, \\ i\dot{U}_B &= V^* \exp \left[ -i \int_0^t [W_A(t') - W_B(t')] dt' \right] U_A. \end{aligned} \quad (22)$$

Equations (22) can be recast in the form

$$\ddot{U}_B + i(W_A - W_B)\dot{U}_B + V^2 U_B = 0. \quad (23)$$

Making the substitution

$$U_B = R_B \exp \left[ -\frac{i}{2} \int_0^t [W_A(t') - W_B(t')] dt' \right] \quad (24)$$

and rearranging, we obtain

$$\ddot{R}_B + \left[ V^2 + \frac{W^2(t)}{4} - \frac{i\dot{W}(t)}{2} \right] R_B = 0, \quad (25)$$

with  $W(t) = W_A(t) - W_B(t)$ , which has to be integrated for the different regimes of collision considered.

### C. The weak-field regime

We label weak-field regime for microwave-assisted radiative collisions the case where

$$W(F_s) > \frac{dW}{dF} \Big|_{F_s} F_{mw} > \frac{d^2W}{dF^2} \Big|_{F_s} F_{mw}^2, \quad (26)$$

which means, as shown in Fig. 11, that the microwave field amplitude is less than the static field. An important implication of this restriction is that the weak-field description does not apply to the case of zero static field. We assume also that

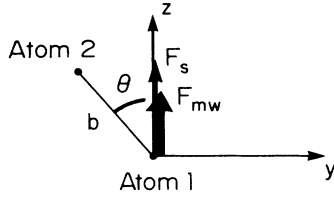


FIG. 16. Geometry of the collision of two atoms. Atom 1 is at rest at the origin. Atom 2 is moving in the  $x$  direction, perpendicular to the paper with velocity  $v$  and impact parameter  $b$ . At  $x=0$ , the plane of the paper, the vector from atom 1 to atom 2 makes an angle  $\theta$  with the  $z$  axis, the axis of quantization. The static  $F_s$  and microwave  $F_{mw}$  electric fields are parallel to the direction  $z$ .

$$W^2(F_s) \gg 4V^2. \quad (27)$$

We shall see that this condition means that the duration of one collision is long compared to the microwave period. If these conditions are met, Eq. (25) can be written

$$\ddot{R}_B + \frac{1}{4} \left[ \left[ W(F(t)) + \frac{2V^2}{W(F_s)} \right]^2 - 2i\dot{W}(F(t)) \right] R_B = 0. \quad (28)$$

By assuming a solution of the form

$$P(F_s, F_{mw}) \approx V^2 \left| \int_0^{2b/v} \exp \left[ -i \left[ W(F_s) + \frac{1}{4} \frac{d^2W}{dF^2} \Big|_{F_s} F_{mw}^2 + \frac{2V^2}{W(F_s)} \right] t - i \frac{dW}{dF} \Big|_{F_s} \frac{F_{mw}}{\omega_{mw}} \sin(\omega_{mw}t + \phi) \right] dt \right|^2, \quad (33)$$

where  $\phi$  is a phase characterizing the phase of the microwave field at the beginning of one collision. This phase changes randomly from one collision to another. Using a Floquet development we can write

$$P(F_s, F_{mw}) \approx V^2 \left| \sum_{m=-\infty}^{+\infty} (-1)^m J_m \left[ \frac{dW}{dF} \Big|_{F_s} \frac{F_{mw}}{\omega_{mw}} \right] \times \int_{\phi/\omega_{mw}}^{2b/v + \phi/\omega_{mw}} \exp -i \left[ \left[ W(F_s) + \frac{1}{4} \frac{d^2W}{dF^2} \Big|_{F_s} F_{mw}^2 + \frac{2V^2}{W(F_s)} \right] \left[ t - \frac{\phi}{\omega_{mw}} \right] - m\omega_{mw}t \right] dt \right|^2. \quad (34)$$

Evaluating the integral we get

$$P(F_s, F_{mw}) \approx V^2 \left| \sum_{m=-\infty}^{+\infty} (-1)^m e^{im\phi} J_m \left[ \frac{dW}{dF} \Big|_{F_s} \frac{F_{mw}}{\omega_{mw}} \right] \times i \frac{\exp \left[ -i \left[ W(F_s) + \frac{1}{4} \frac{d^2W}{dF^2} \Big|_{F_s} F_{mw}^2 + \frac{2V^2}{W(F_s)} - m\omega_{mw} \right] \frac{2b}{v} \right] - 1}{W(F_s) + \frac{1}{4} \frac{d^2W}{dF^2} \Big|_{F_s} F_{mw}^2 + \frac{2V^2}{W(F_s)} - m\omega_{mw}} \right|^2. \quad (35)$$

To calculate the total cross section, we must integrate the probability  $P$  over the impact parameter  $b$  and average over all the initial phases  $\phi$  of the microwave field to account for the random times of the collisions. Formally,

$$\sigma(F_s, F_{mw}) = \frac{1}{2\pi} \int_0^{2\pi} d\phi \int_0^\infty 2\pi b db P(F_s, F_{mw}, b). \quad (36)$$

$$R_B(t) = A(t) \exp \left[ \frac{i}{2} \int_0^t \{ W(F(t')) + [2V^2/W(F_s)] \} dt' \right], \quad (29)$$

we get

$$\ddot{A}(t) + i \left[ W(F(t)) + \frac{2V^2}{W(F_s)} \right] \dot{A}(t) = 0 \quad (30)$$

and

$$\dot{A}(t) = \dot{A}(0) \int_0^t \exp \left[ -i \int_0^{t'} \left[ W(F(t'')) + \frac{2V^2}{W(F_s)} \right] dt'' \right] dt', \quad (31)$$

with  $\dot{A}(0) = \dot{C}_B(0) = -iV$ .

The probability of finding the atoms in the two  $p$  states is given by

$$P(F_s, F_{mw}) = \left| C_B \left[ \frac{2b}{v} \right] \right|^2 = \left| A \left[ \frac{2b}{v} \right] \right|^2. \quad (32)$$

Thus we may write the probability as

Explicitly,

$$\sigma(F_s, F_{mw}) = 2\pi \int_0^\infty \frac{\chi^2}{b^5} \sum_m J_m^2 \left[ \frac{dW}{dF} \Big|_{F_s} \frac{F_{mw}}{\omega_{mw}} \right] \left[ \frac{\sin \left[ \frac{1}{2} \left[ E_m + \frac{2\chi^2}{W(F_s)b^6} \right] \frac{2b}{v} \right]}{\frac{1}{2} \left[ E_m + \frac{2\chi^2}{W(F_s)b^6} \right]} \right]^2 db, \quad (37)$$

with

$$E_m = W(F_s) + \frac{1}{4} \frac{d^2W}{dF^2} \Big|_{F_s} F_{mw}^2 - m\omega_{mw}. \quad (38)$$

This cross-section expression permits us to calculate in the weak-field regime the cross section of one-, two-, . . . microwave-photon-assisted radiative collision processes but does not give any information about the relation to the case of zero-photon-assisted collisions, the resonant collisions observed without microwaves. The treatment of radiative collisions developed here is similar to that developed in Ref. 15 but is applied to the case of microwave-assisted collisions.

We note that the cross section is approximately equal to zero, except for the value of  $F_s$  such that

$$E_m \approx 0 \quad (\text{with } m \neq 0).$$

Under these conditions, we see that the collision process should exhibit resonances for the values of the energy, such that

$$W(F_s) = m\omega_{mw} - \frac{1}{4} \frac{d^2W}{dF^2} \Big|_{F_s} F_{mw}^2 \quad (m \neq 0), \quad (39)$$

$$\sigma^{(m)}(F_s, F_{mw}) \approx 2\pi J_m^2 \left[ \frac{dW}{dF} \Big|_{F_s} \frac{F_{mw}}{\omega_{mw}} \right] \int_0^\infty \frac{\chi^2}{b^5} \left[ \frac{\sin \left[ \frac{1}{2} \left[ E_m + \frac{2\chi^2}{W(F_s)b^5} \right] \frac{2b}{v} \right]}{\frac{1}{2} E_m + \frac{2\chi^2}{W(F_s)b^6}} \right]^2 db. \quad (42)$$

We can calculate its value at resonance ( $E_m = 0$ )

$$\sigma_M^{(m)}(F_{mw}) \approx 10.79\chi^{6/5}v^{-8/5}W(F_s)^{2/5}J_m^2 \left[ \frac{dW}{dF} \Big|_{F_s} \frac{F_{mw}}{\omega_{mw}} \right], \quad (43)$$

which can also be written

$$\sigma_M^{(m)}(F_{mw}) \approx 10.79\chi^{6/5}v^{-8/5}W(F_s)^{2/5} \times \left[ \frac{1}{m!} \left[ \frac{1}{2} \frac{dW}{dF} \Big|_{F_s} \frac{F_{mw}}{\omega_{mw}} \right]^m \right]^2. \quad (44)$$

The expression of Eq. (44) is very similar to that obtained in Ref. 15 for laser-induced collisional energy transfers in the weak-field regime.

(c) *Shape of the resonance:* In particular, the asymmetrical line shape of laser-assisted collisions is found again for microwave-assisted collisions. Such a result is not surprising because our treatment of the weak-field regime is similar to that developed in Ref. 15. We can see that

which corresponds to the  $m$ -microwave-photon-assisted radiative collision process.

We can analyze the main characteristics of these processes.

(a) *Shift of the resonance:* The resonance position exhibits an ac Stark shift  $\Delta$  from the position corresponding to a microwave field amplitude equal to zero:

$$W(F_s) = E_{np}(F_s) + E_{(n-1)p}(F_s) - 2E_{ns}(F_s) = m\omega_{mw}. \quad (40)$$

The value of this shift is given by

$$\Delta = -\frac{1}{4} \frac{d^2W}{dF^2} \Big|_{F_s} F_{mw}^2 = -\frac{1}{4} \left[ \frac{d^2E_{np}}{dF^2} \Big|_{F_s} + \frac{d^2E_{(n-1)p}}{dF^2} \Big|_{F_s} - 2 \frac{d^2E_{ns}}{dF^2} \Big|_{F_s} \right] F_{mw}^2. \quad (41)$$

It is proportional to the square of the amplitude of the microwave field, i.e., proportional to the microwave energy.

(b) *Maximum cross-section:* The cross section of  $m$ -microwave-photon-assisted radiative collision is given by

the cross section of Eq. (42) is not symmetric about  $E_m = 0$ . The cross section is larger for  $E_m$  and  $W(F_s)$  of opposite sign, and we can show that the slowly decreasing side varies as  $E_m^{1/2}$ .

#### D. The strong-field regime

We label strong-field regime the case where

$$\frac{dW}{dF} \Big|_{F_s} F_{mw} > W(F_s). \quad (45)$$

We assume also that

$$W^2(F) \gg 4V^2. \quad (46)$$

If these conditions are met Eq. (25) can be written

$$\ddot{R}_B + \frac{1}{4} [W(F(t))^2 - 2i\dot{W}(F(t))]R_B = 0, \quad (47)$$

and the probability of finding the atoms in the two  $p$  states is given by

$$P(F_s, F_{mw}) \approx V^2 \left| \int_0^{2b/v} \exp \left[ \int_0^t -iW(F(t')) dt' \right] dt \right|^2 \quad (48)$$

which can be written in a Floquet development as

$$P(F_s, F_{mw}) \approx V^2 \left| \sum_{m=-\infty}^{+\infty} (-1)^m J_m \left[ \frac{dW}{dF} \right]_{F_s, \omega_{mw}} \left[ \frac{F_{mw}}{\omega_{mw}} \right] \int_0^{2b/v} \exp -i \left[ W(F_s) + \frac{1}{4} \frac{d^2W}{dF^2} \right]_{F_s} F_{mw}^2 - m\omega_{mw} \right] t dt \right|^2. \quad (49)$$

As for the weak-field-regime case we note that the probability  $P$  is different from zero when

$$E_m = W(F_s) + \frac{1}{4} \frac{d^2W}{dF^2} \Big|_{F_s} F_{mw}^2 - m\omega_{mw} \approx 0. \quad (50)$$

Note that the resonances are shifted from their expected positions by the ac Stark shift of

$$\left[ -\frac{1}{4} \frac{d^2W}{dF^2} \Big|_{F_s} F_{mw}^2 \right].$$

As long as the collisional resonances do not overlap the resonance condition of Eq. (50) allows us to separate the contributions to the probability of Eq. (49) from different values of  $m$ . Thus the probability of Eq. (49) may be rewritten as a sum of probabilities  $P^{(m)}(F_{mw}, b)$ , and for the resonance corresponding to the process assisted by  $m$  microwave photons, we get

$$\begin{aligned} P^{(m)}(F_{mw}, b) &\approx V^2 J_m^2 \left[ \frac{dW}{dF} \Big|_{F_s, \omega_{mw}} \left[ \frac{F_{mw}}{\omega_{mw}} \right] \right] \frac{4b^2}{v^2} \\ &\approx \frac{4\chi^2}{b^4 v^2} J_m^2 \left[ \frac{dW}{dF} \Big|_{F_s, \omega_{mw}} \left[ \frac{F_{mw}}{\omega_{mw}} \right] \right]. \end{aligned} \quad (51)$$

To calculate the total cross section at resonance for the  $m$ -microwave-photon-assisted process we must integrate the probability  $P^{(m)}$  over impact parameter  $b$ . In fact, it is clear that the probability  $P^{(m)}$  cannot be larger than 1, which defines an impact parameter  $b_m(F_{mw})$ :

$$b_m^2(F_{mw}) = \frac{2\chi J_m \left[ \frac{dW}{dF} \Big|_{F_s, \omega_{mw}} \left[ \frac{F_{mw}}{\omega_{mw}} \right] \right]}{v}. \quad (52)$$

In fact, an exact numerical integration of the Eqs. (16) for strong-field-regime conditions shows (see Fig. 17) that Eq. (51) is a relatively good approximation for  $b > b_m$  but that for  $b < b_m$  the probability  $P^{(m)}$  exhibits rapid oscillations, which permits us to approximate  $P^{(m)}$  by  $\frac{1}{2}$  in this zone. In the solid curves of Fig. 17 we show the collision probabilities for resonant collision and collisions assisted by microwaves obtained by numerical integration of Eq. (16). For the resonant-collision case we also show the approximate expression of Eq. (48). For the collisions assisted by microwaves we note that the last maximum,  $P^{(m)}(F_{mw}) = 1$  occurs at the point

$$b_m(F_{mw}) = b_0 \left[ J_m \left[ \frac{dW}{dF} \Big|_{F_s^{(m)}, \omega_{mw}} \left[ \frac{F_{mw}}{\omega_{mw}} \right] \right] \right]^{1/2}. \quad (53)$$

Note that similar behavior is obtained for the cases of

$m = 1, 2,$  and  $3$ , i.e., for one, two, or three microwave-photon-assisted collisions. These considerations lead us to give an approximate expression for the cross section  $\sigma_M^{(m)}$  in the strong-field regime:

$$\sigma_M^{(m)}(F_{mw}) \approx \pi b_m^2 + \int_{b_m}^{+\infty} 2\pi b P^{(m)}(F_{mw}, b) db, \quad (54)$$

$$\sigma_M^{(m)}(F_{mw}) \approx 2\pi b_m^2(F_{mw}), \quad (55)$$

$$\sigma_M^{(m)}(F_{mw}) \approx 2\pi b_0^2(0) J_m \left[ \frac{dW}{dF} \Big|_{F_s, \omega_{mw}} \left[ \frac{F_{mw}}{\omega_{mw}} \right] \right], \quad (56)$$

$$\sigma_M^{(m)} \approx \frac{4\pi\chi}{v} J_m \left[ \frac{dW}{dF} \Big|_{F_s, \omega_{mw}} \left[ \frac{F_{mw}}{\omega_{mw}} \right] \right], \quad (57)$$

where  $b_0(0)$  is the impact parameter for resonant collisions in the absence of microwaves. A better expression can be obtained by considering the curves of calculated probabilities given by Fig. 17. All these curves look similar to the probability curve of resonant collisions without microwaves but, at least in first approximation, with a compression versus the impact parameter  $b$  by a ratio

$$\left[ J_m \left[ \frac{dW}{dF} \Big|_{F_s, \omega_{mw}} \left[ \frac{F_{mw}}{\omega_{mw}} \right] \right] \right]^{1/2}.$$

This leads for the cross section to the expression

$$\sigma_M^{(m)}(F_{mw}) \approx \sigma_M^{(0)}(0) J_m \left[ \frac{dW}{dF} \Big|_{F_s, \omega_{mw}} \left[ \frac{F_{mw}}{\omega_{mw}} \right] \right]. \quad (58)$$

An exact expression for the resonant-collision cross section in the absence of microwaves can be calculated. We find for the probability  $P^{(0)}(0, b)$ ,

$$P^{(0)}(0, b) = \sin^2 \left[ \frac{2\chi}{vb^2} \right]. \quad (59)$$

We note that we get exactly the same expression for  $\sigma_M^{(0)}(0)$  by taking for the matrix element  $V$  the expression given by Eq. (18). We can show that

$$\sigma_M^{(0)}(0) = \int_0^\infty 2\pi b \sin^2 \left[ \frac{2\chi}{vb^2} \right] db = \frac{\pi^2\chi}{v}. \quad (60)$$

The impact parameter  $b_0(0)$  for resonant collisions, for which  $P^{(0)}(0, b) = 1$ , is readily determined from Eq. (59);

$$b^2(0) = \frac{4\chi}{v\pi}, \quad (61)$$

which leads to the impact parameters  $b_m(F_{mw})$  for radiative collisions:

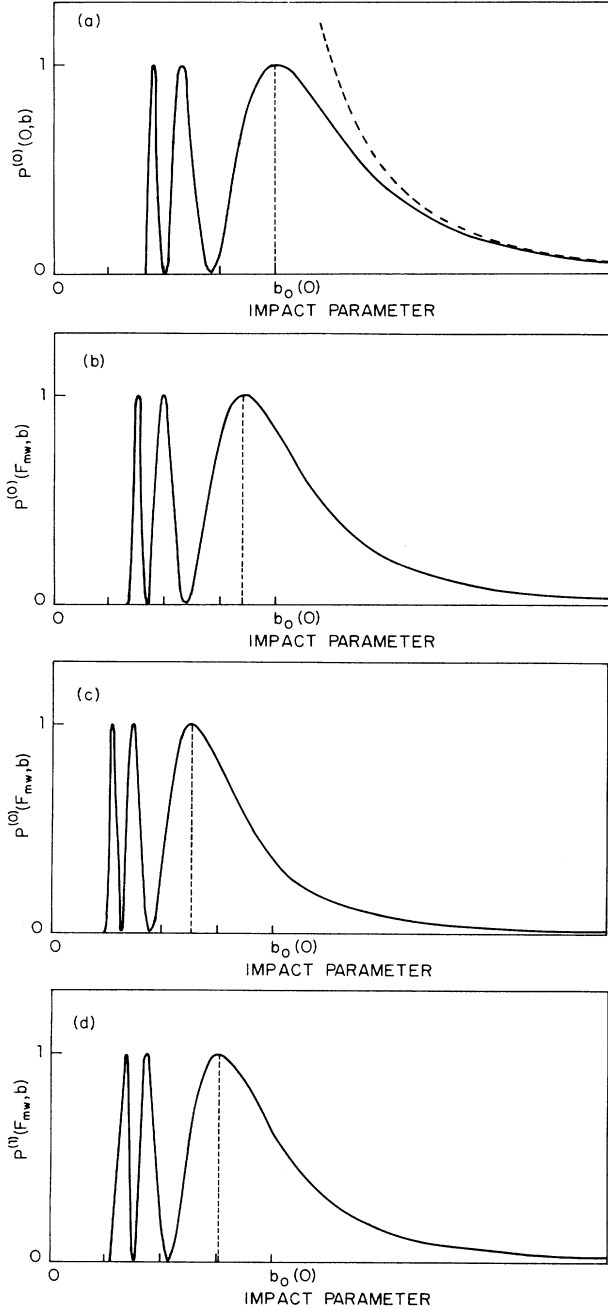


FIG. 17. Typical calculated curves corresponding to transition probabilities  $P^{(m)}(F_{mw}, b)$  vs impact parameter  $b$ : (a)–(c) in the case of resonant collision process for respective values of the parameter

$$\left[ \frac{dW}{dF} \right]_{F_s^{(0)} \omega_{mw}} \frac{F_{mw}}{F_s \omega_{mw}}$$

equal to 0 (no microwaves), 1.1, and 3.85. The dotted line in (a) corresponds to the asymptotic behavior in  $4\chi^2/b^4 v^2$  given by Eq. (51) for large impact parameter  $b$ . (d) In the case of the one-microwave-photon-assisted radiative collision process for a value of the parameter

$$\left[ \frac{dW}{dF} \right]_{F_s^{(1)} \omega_{mw}} \frac{F_{mw}}{F_s \omega_{mw}}$$

equal to 1.85.

$$b_m^2(F_{mw}) = \frac{4\chi}{v\pi} J_m \left[ \frac{dW}{dF} \right]_{F_s \omega_{mw}} \frac{F_{mw}}{F_s \omega_{mw}}. \quad (62)$$

Before comparing these cross sections to the measurements a few remarks are in order. First the coherence of the different processes shown in Fig. 13 is automatically taken into account by the use of  $dW/dF$  in the argument of the Bessel function. Consider for illustration the situation shown in Fig. 13 in which the  $s$  state has no sidebands, or equivalently negligible Stark shift (the same reasoning may be extended to include the  $ns$  state Stark shift). In this case,

$$\frac{dW}{dF} = \frac{dE_{np}}{dF} + \frac{dE_{(n-1)p}}{dF}; \quad (63)$$

using the Bessel function identity we can rewrite the Bessel function in the cross section of Eqs. (56), (57), and (62), as

$$J_m \left[ \frac{dW}{dF} \right]_{F_s \omega_{mw}} \frac{F_{mw}}{F_s \omega_{mw}} = \sum_{k=-\infty}^{\infty} J_{m-k} \left[ \frac{dE_{np}}{dF} \right]_{F_s \omega_{mw}} \frac{F_{mw}}{F_s \omega_{mw}} \times J_k \left[ \frac{dE_{(n-1)p}}{dF} \right]_{F_s \omega_{mw}} \frac{F_{mw}}{F_s \omega_{mw}}, \quad (64)$$

that is, as a coherent sum over those processes which correspond to the net absorption of  $m$  photons. Although the different processes could be summed, it is evidently easier to treat the problem globally and have the sum done automatically. Finally we remark that Eq. (64) incorporates the interference between different collisional processes, which, depending upon the phase, can be constructive or destructive. It is interesting to note this unusual and explicitly observable collisional effect.

Thus far we have focused on the case in which the duration of one collision is much longer than the microwave period. This condition, with the further restrictions of Eqs. (27) and (46), has allowed us to describe radiative collisions in terms of resonant collisions between “microwave dressed” atoms. The case in which the duration of one collision becomes much shorter than the microwave period is also of interest. In this situation, the radiative collision process should be treated as a resonant-collision process at a well-defined value of the microwave field, and therefore of the total field  $F$ . The total cross section of a resonant collision can be written

$$\sigma(W(F)) = \sigma_0 f(W(F)), \quad (65)$$

where  $f(W(F))$  is a function characterizing the width and the shape of the observed collisional resonance and which satisfies

$$f(0) = 1. \quad (66)$$

In the presence of microwaves the total cross section becomes

$$\sigma(W(F_s)) = \frac{\omega}{2\pi} \int_0^{2\pi/\omega} \sigma_0 f(W[F_s + F_{mw} \sin(\omega_{mw} t)]) dt. \quad (67)$$

Figure 18(c) shows the general behavior of a collisional resonance in the presence of a low-frequency field. The resonant-collision line is split into two asymmetric lines, the splitting proportional to the microwave field amplitude. From Eq. (67) it is apparent that the cross section is a time average, and since more time is spent at the extrema of the oscillating field, they dominate the cross section.

#### IV. THEORY-EXPERIMENT COMPARISON AND CONCLUSION

The experimental data reported in Sec. II of this article permit us to analyze three kinds of parameters: the width or the shape of the resonance lines, the shift of the collision resonance, and the cross sections of the different collisional processes.

Concerning the width of the resonance in the strong-field regime, from Eqs. (49) and (52) it is apparent that the width of the resonances is given by (where FWHM represents full width at half maximum)

$$\Delta(\text{FWHM}) = \frac{2\pi\nu}{b_m} = \frac{2\pi\nu}{b_0} J_m^{-1/2} \left[ \frac{dW}{dF} \Big|_{F_s} \frac{F_{\text{mw}}}{\omega_{\text{mw}}} \right]. \quad (68)$$

As the square root of the Bessel function

$$J_m \left[ \frac{dW}{dF} \Big|_{F_s} \frac{F_{\text{mw}}}{\omega_{\text{mw}}} \right]$$

does not exhibit, in the strong-field regime, significant variation, the theoretical widths of resonances are relatively constant versus the microwave field, in agreement with our experimental data.

The calculated cross sections of Eqs. (56), (57), and (62) exhibit no asymmetry, whereas the experimental cross

sections most certainly do. We note though that the experimental asymmetry is present even in the zero-photon or resonant-collision signals as shown by Fig. 7. The  $(0,0)^0$  resonance is degraded to the high-field side, whereas the  $(1,1)^0$  resonance is degraded to the low-field side. Inspection of Fig. 7 shows that this persists for the  $(0,0)^m$  and  $(1,1)^m$   $m$ -photon resonances as well. The asymmetry is thus not peculiar to the presence of the microwave photons, but is due to our neglect of the variation of interatomic potential with distance. As mentioned earlier, this variation is due to nonresonant coupling to other states.

Actually the addition of the microwaves may be a useful way of studying the interatomic potentials. As shown by Eq. (62), the impact parameter for a radiative collision is controlled by the strength of the microwave field. The linewidth of the collisional resonance scales as  $1/b_m(F_{\text{mw}})$ , but more important, the region of the interatomic potential responsible for the collisional resonance depends on the microwave field. For example, at very low microwave powers the one-photon resonances should be broad and are due mostly to interactions occurring at small separations of the colliding atoms where the interatomic potential is most likely not to be flat. At higher powers, where

$$J_1 \left[ \frac{dW}{dF} \Big|_{F_s} (1) \frac{F_{\text{mw}}}{\omega_{\text{mw}}} \right] \sim 1,$$

the impact parameter is larger, and the interatomic potential is essentially flat, leading to sharper, more symmetric resonances. This development with microwave power is in fact quite clearly observed, as shown by Fig. 7.

Alternatively, the very asymmetric profiles observed in the weak-field regime [as shown in Figs. 7(b)–(d)] can be interpreted in the weak-field formalism developed in Sec. III B. However, overlap between the different radiative collision processes does not permit a quantitative investigation of these data. In particular, it has not been possible to test the  $E_m^{-1/2}$  dependence of the resonance shape.

Concerning the shift observed for the radiative collision resonance (as those shown in Fig. 8), in the weak- and strong-field-regime theory the resonance position exhibits an ac Stark shift [see Eqs. (41) and (50)] of

$$\left[ -\frac{1}{4} \frac{d^2W}{dF^2} \Big|_{F_s} F_{\text{mw}}^2 \right].$$

Assuming that the energy-level curves of  $ns$  and  $np$  levels can be approximated by parabolic curves (which is a good approximation), it is easy to show that the ac Stark shift, expressed in terms of the change in the static field at which the resonance is observed, is given by

$$\Delta = F_{\text{mw}}^2 / 4F_s^{(m)}. \quad (69)$$

Recalling that 1 W of microwave input power corresponds to 95 V/cm, we can use Eq. (69) to predict slopes of 6.4, 7.4, and 8.7 V/cm W for, respectively, the one-, two-, and three-microwave-photon-assisted radiative collision processes. These values are in good agreement with the experimental data of 6.8(4), 6.5(4), and 8.9(5) V/cm W.

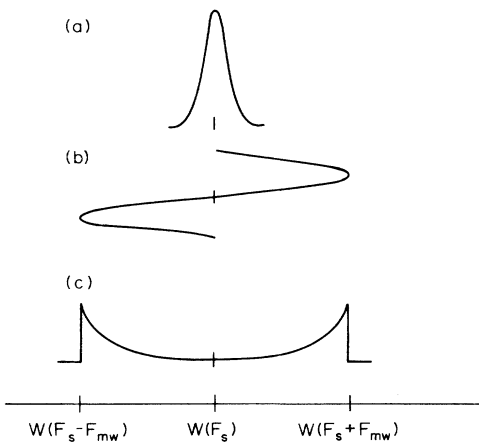


FIG. 18. Collisions in the presence of a low-frequency microwave field. (a) the resonant collision profile without the microwaves. (b) One period of microwave field showing both the amplitude and the time weighting of the extreme field values. (c) Typical weighted shape of radiative collision line when the microwave period becomes long compared to the duration of one collision.

In the theory we have considered separately the cases of the weak- and the strong-field regimes. Figure 9 shows the theoretical relative cross sections of the different radiative collision processes versus the microwave electric field and the corresponding experimental data. The strong-field regime curves,

$$\sigma^m \propto \left| J_m \left[ \frac{dW}{dF} \right]_{F_s} (m) \frac{F_{\text{mw}}}{\omega_{\text{mw}}} \right|^2,$$

are obviously not physically significant in the weak-field regime, and more generally when the cross sections are near zero (shown by the dotted line of Fig. 9). In the weak-field region the cross section is given by the expression of Eq. (44). We have used the actual values of the average collision velocity,  $\bar{v} = 1.6 \times 10^{-4}$ , and dipole moments  $\mu_1 = \mu_2 = 0.6n^{*2}$ . Here,  $n^{*2}$  is the effective quantum number of the  $ns$  state of binding energy  $W = -1/2n^{*2}$ . The weak-field-regime curves (short-dashed line) meet the strong-field-regime curves at the points of transition between both regimes for the different radiative collisional processes. It is clear that the passage from one regime to the other cannot be abrupt but must be smooth. Figure 19 shows the theoretical cross-section curves versus the microwave field in the cavity. The agreement between these curves and the plotted experimental points is generally good. In particular, the zeros of the experimental cross sections are reproduced in the theory.

There is, however, one discrepancy. The data of Fig. 9 are normalized so that the resonant-collision cross section for no microwave field is 2.00, in disagreement with the theoretical value of 1. In our preliminary analysis of the data<sup>18</sup> we used a simpler perturbative treatment in which the cross sections are given by the squares of Bessel functions, leading to smaller theoretical radiative collision cross sections, in better agreement with the experiments. A more thorough analysis has shown that the simple perturbative approach should not be valid, and we have thus developed the approach presented here. There are, in fact, several experimental difficulties which may have contributed to the normalization discrepancy. The overlap between the different radiative collisional processes makes it difficult to measure these cross sections unambiguously. Accurate determination of the zeroes in the cross section is difficult because of the background signal due to the blackbody radiative transfer.<sup>36</sup> The narrow width of the collisional resonances also contributes to uncertainties in the determination of their maxima. These factors may well explain a systematic error in the measurement which would have led to the discrepancy of the resonant-collision signal at zero microwave field.

The low-frequency assumption has permitted us to develop a useful formalism to describe the behavior of Ryd-

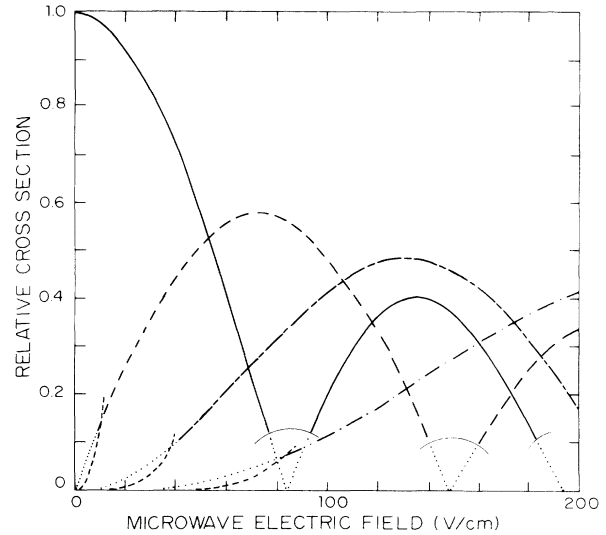


FIG. 19. Theoretical cross-section variation vs microwave field amplitude corresponding to the experimental data of Fig. 9. Strong-field regime, cross sections:  $(0,0)^0$  (—),  $(0,0)^1$  (---),  $(0,0)^2$  (- - - -) and  $(0,0)^3$  (- · - · -). Parts of curves where the strong-field-regime theory is not valid are dotted lines. Weak-field-regime cross sections are represented by short dashed lines for the processes  $(0,0)^1$ ,  $(0,0)^2$ , and  $(0,0)^3$ .

berg states isolated from the other states of the manifold, in the presence of microwave field in a weak- and a strong-field regime. In particular, microwave-assisted radiative collisions can be treated as resonant collisions between “microwave dressed” Rydberg atoms, and the comparison of these theoretical results with those obtained experimentally supports the validity of our treatment. The relative simplicity of this treatment and the possibility of nearly exact calculations (by using, for instance, a better interatomic potential) for radiative collisions lead to the conclusion that microwave-assisted radiative collisions between dressed atoms comprise a good system in which to analyze some of the general properties of radiative collision processes. More generally, Rydberg atoms in the presence of microwaves offer the possibility of investigating a variety of physical problems relating to the interaction of matter with radiation.<sup>37</sup> The specific attraction is that a whole range of parameters can be studied in a more quantitative fashion than is possible to do otherwise.

#### ACKNOWLEDGMENT

This work has been supported by the U.S. Air Force Office of Scientific Research under Grant No. AFOSR-87-0007.

\*Permanent address: Department of Physics, University of Connecticut, Storrs, CT 06268.

<sup>1</sup>L. I. Gudzenko and S. S. Yakovlenko, Zh. Eksp. Teor. Fiz. **62**, 1686 (1972) [Sov. Phys.—JETP **35**, 877 (1972)].

<sup>2</sup>A. Gallagher and T. Holstein, Phys. Rev. A **16**, 2413 (1977).

<sup>3</sup>R. W. Falcone, W. R. Green, J. C. White, J. F. Young, and S. E. Harris, Phys. Rev. A **15**, 1333 (1977).

<sup>4</sup>P. Cahuzac and P. E. Toschek, Phys. Rev. Lett. **40**, 1087

- (1978).
- <sup>5</sup>A. V. Hellfeld, J. Caddick, and J. Weiner, *Phys. Rev. Lett.* **40**, 1369 (1978).
- <sup>6</sup>W. R. Green, M. D. Wright, J. Lukasik, J. F. Young, and S. E. Harris, *Opt. Lett.* **4**, 265 (1979).
- <sup>7</sup>J. C. White, *Opt. Lett.* **6**, 242, (1981).
- <sup>8</sup>W. R. Green, J. Lukasik, J. R. Wilson, M. D. Wright, J. F. Young, and S. E. Harris, *Phys. Rev. Lett.* **42**, 920 (1979).
- <sup>9</sup>S. E. Harris and D. B. Lidow, *Phys. Rev. Lett.* **33**, 674 (1974).
- <sup>10</sup>S. Geltman, *J. Phys. B* **9**, L569 (1976).
- <sup>11</sup>P. L. Knight, *J. Phys. B* **10**, L195 (1977).
- <sup>12</sup>S. I. Yakovlenko, *Kvant. Elektron. (Moscow)* **5**, 259 (1978) [*Sov. J. Quantum Electron.* **8**, 151 (1978)].
- <sup>13</sup>M. G. Payne, V. E. Anderson, and J. E. Turner, *Phys. Rev. A* **20**, 1032 (1979).
- <sup>14</sup>E. J. Robinson, *J. Phys. B* **12**, 1451 (1979); **13**, 2359 (1980).
- <sup>15</sup>S. E. Harris and J. C. White, *IEEE J. Quantum Electron.* **QE-13**, 972 (1977).
- <sup>16</sup>J. Lukasik and S. C. Wallace, *Phys. Rev. Lett.* **47**, 240 (1981).
- <sup>17</sup>R. Kachru, N. H. Tran, and T. F. Gallagher, *Phys. Rev. Lett.* **49**, 191 (1982).
- <sup>18</sup>P. Pillet, R. Kachru, N. H. Tran, W. W. Smith, and T. F. Gallagher, *Phys. Rev. Lett.* **50**, 1763 (1983).
- <sup>19</sup>R. Kachru, T. F. Gallagher, F. Gounand, P. Pillet, and N. H. Tran, *Phys. Rev. A* **28**, 2676 (1983).
- <sup>20</sup>T. H. Jeys, G. B. McMillan, K. A. Smith, F. B. Dunning, and R. F. Stebbings, in *Proceedings of the Twelfth International Conference on the Physics of Electronic and Atomic Collisions*, edited by S. Datz (North-Holland, Amsterdam, 1982), p. 1107.
- <sup>21</sup>K. A. Smith, F. G. Kellert, R. D. Rundel, F. B. Dunning, and R. F. Stebbings, *Phys. Rev. Lett.* **40**, 1362 (1978).
- <sup>22</sup>T. F. Gallagher, G. A. Ruff, and K. A. Safinya, *Phys. Rev. A* **22**, 843 (1980).
- <sup>23</sup>K. A. Safinya, J. F. Delpach, F. Gounand, W. Sandner, and T. F. Gallagher, *Phys. Rev. Lett.* **47**, 405 (1981).
- <sup>24</sup>T. F. Gallagher, K. A. Safinya, F. Gounand, J. F. Delpach, W. Sandner, and R. Kachru, *Phys. Rev. A* **5**, 1905 (1982).
- <sup>25</sup>T. F. Gallagher, L. M. Humphrey, W. E. Cooke, R. M. Hill, and S. A. Edelstein, *Phys. Rev. A* **25**, 1098 (1977).
- <sup>26</sup>P. Pillet, H. B. van Linden van den Heuvell, W. W. Smith, R. Kachru, N. H. Tran, and T. F. Gallagher, *Phys. Rev. A* **30**, 280 (1984).
- <sup>27</sup>C. H. Townes and A. L. Schawlow, *Microwave Spectroscopy* (McGraw-Hill, New York, 1955), and references therein.
- <sup>28</sup>C. Brechnignac, Ph. Cahuzac, and P. E. Toschek, *Phys. Rev. A* **21**, 1969 (1980).
- <sup>29</sup>S. H. Autler and C. H. Townes, *Phys. Rev.* **100**, 703 (1955).
- <sup>30</sup>P. Pillet, W. W. Smith, R. Kachru, N. H. Tran, and T. F. Gallagher, *Phys. Rev. Lett.* **50**, 1042 (1983).
- <sup>31</sup>N. F. Mott and H. S. W. Massey, *The Theory of Atomic Collisions* (Clarendon, Oxford, 1950).
- <sup>32</sup>P. W. Anderson, *Phys. Rev.* **76**, 647 (1949).
- <sup>33</sup>J. van Kranendonk, *Can. J. Phys.* **41**, 433 (1963).
- <sup>34</sup>T. Oka, in *Advances in Atomic and Molecular Physics*, edited by D. R. Bates and I. Esterman (Academic, New York, 1973), Vol. 9.
- <sup>35</sup>P. L. Houston, in *Photoselective Chemistry*, Part 2, edited by J. Jortner (Wiley, New York, 1981).
- <sup>36</sup>W. E. Cooke and T. F. Gallagher, *Phys. Rev. A* **21**, 588 (1980).
- <sup>37</sup>S. Haroche, in *New Trends in Atomic Physics*, Proceedings of the Les Houches Summer School in Theoretical Physics, edited by G. Grynberg and R. Stora (North-Holland, Amsterdam, 1984), Vol. I, and references therein.